

Designing Transcranial Magnetic Stimulation Systems

Kent Davey, *Fellow, IEEE*, and Mark Riehl

Abstract—We explain the process of designing optimized transcranial magnetic stimulation systems and outline a method for identifying optimal system parameters such as the number of turns, the capacitor size, the working voltage, and the size of the stimulation coil. The method combines field analysis, linear and nonlinear circuit analysis, and neural strength–duration response parameters. The method uses boundary-element analysis to predict the electric field as a function of depth, frequency, current, and excitation coil size. It then uses the field analysis to determine the inductance as a function of size and, in general, current when a saturable core is used. Circuit analysis allows these electric field computations to be indexed against system parameters, and optimized for total system energy and stimulation coil size. System optimizations depend on desired stimulation depth. A distinguishing feature of the method is that it inherently treats excitation frequency as an unknown to be determined from optimization.

Index Terms—Capacitance, core, energy, iron, neural, stimulation.

I. INTRODUCTION

THE usefulness of magnetic field stimulation devices for the stimulation of neurons is well established, and considerable research has been directed to identifying appropriate coil shapes and efficiencies to minimize stimulation energy. After testing over 16 000 coil designs, Durand concludes that a clover leaf design is optimal for infinitely long fibers, whereas a butterfly coil is preferred for bent fibers [1]. Ravazzani gives attention to the skin and proximity effect losses within air coil systems, and recommends large diameter small cross-section coils to mitigate these losses [2]. Onuki performs an optimization to increase induced E using a three-coil setup [3]. A genetic algorithm is employed to change the shape of the coils to maximize the induced field. The pulsewidth was selected *a priori*. Many papers have examined unusual coil designs to enhance focality [4], [5]. This paper outlines a method for optimizing the stimulator system including the stimulator unit.

Among the principle contributions of this paper is the point that this frequency is intimately linked to the stimulation efficiency. It must be treated as an unknown.

Manuscript received May 21, 2004; revised December 1, 2004. This work was supported by Neuronetics, Inc.

K. Davey is with the Center for Electromechanics, University of Texas, Austin, TX 78758 USA (e-mail: k.davey@mail.utexas.edu).

M. Riehl is with Neuronetics, Inc., Malvern, PA 19355 USA (e-mail: mriehl@neuronetics.com).

Digital Object Identifier 10.1109/TMAG.2004.843326

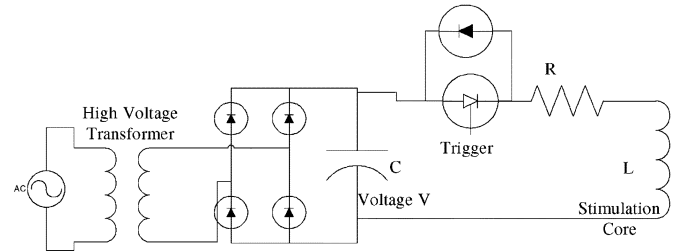


Fig. 1. Typical stimulation circuit.

II. ANALYSIS APPROACH

The cortex is characterized by neural bends and terminations, both of which activate on the electric field, not its gradient. Because of the small conductivity of the cortex, the induced B field is considerably smaller than the source field. For air core stimulators, the magnetic field is dictated entirely by the source current \vec{J}_S . With time harmonic stimulation at frequency ω , the electric field is determined by combining Ampere's law and Faraday's law

$$\nabla \times \nabla \times \vec{E} = j\omega\mu_0\vec{J}_S. \quad (1)$$

The electric field boundary condition $\hat{n} \cdot \vec{E} = 0$ must be imposed to ensure no normal component current exists at the skull interface.

Fig. 1 shows a typical stimulation circuit in which low-voltage ac is transformed to a higher voltage and then rectified. This higher voltage dc charges a capacitor which is fired via a thyristor switch into the stimulator core.

This circuit goes through one complete resonance cycle before the diode thyristor shuts down and further current flow is prohibited by the diode. During the firing cycle, the circuit can be treated as a simple RLC resonance circuit. The current is

$$I(t) = \frac{V}{\omega L} e^{-\alpha t} \sin(\omega t)$$

where

$$\alpha = \frac{R}{2L}$$

$$\omega = \sqrt{\frac{1}{LC} - \alpha^2}. \quad (2)$$

This is the equation for a damped sinusoid. A typical trace with $V = 1.5$ kV, $C = 15$ μ F, $L = 11$ μ H, and $R = 0.2$ Ω is shown in Fig. 2.

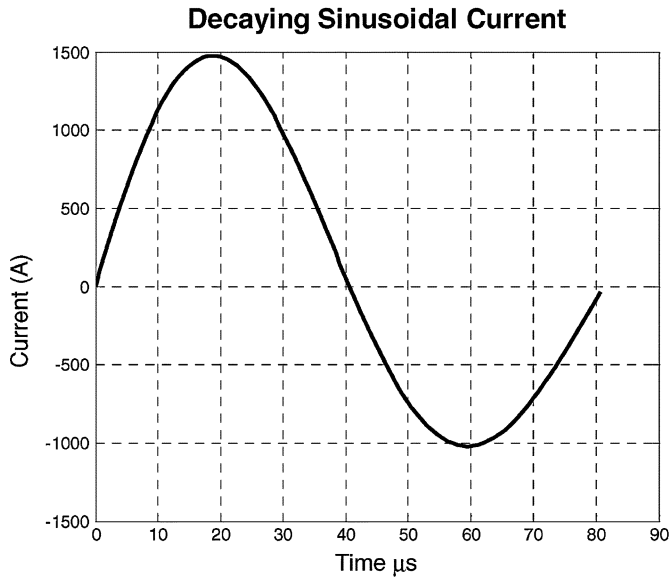


Fig. 2. Characteristic transcranial magnetic stimulation current.

 TABLE I
 NEURAL MAGNETIC STIMULATION RESPONSE PARAMETERS

	Strength Duration Curve Parameters			
	Rheobase (□)		Chronaxie (□)	
	Median (V/m)	Std. Dev. (V/m)	Mean (μs)	Std. Dev. (μs)
Sensory	6.75	2.06	329	78.4
Motor	16	6.1	203	78.5

Of particular interest is the time and value of the current peak

$$t_p = \frac{\tan^{-1}\left(\frac{\omega}{\alpha}\right)}{\omega} \quad (3)$$

$$I_p = V e^{-\left(\frac{\tan^{-1}\left(\frac{\omega}{\alpha}\right)}{\omega/\alpha}\right)} \sqrt{\frac{C}{L}} \quad (4)$$

A. Neural Response

Motor and sensory thresholds for time varying magnetic fields are related to the rheobase and chronaxie strength through strength duration curves. For magnetic stimulation, Geddes reports the rheobase and chronaxie results summarized in Table I [6].

Duration was defined as “onset to zero,” or one-half cycle. In terms of the stimulus frequency f , and the table parameters β and γ , the electric field is

$$E = \beta \cdot (1 + 2\gamma f). \quad (5)$$

Fig. 3 shows the required induced electric field as a function of frequency.

III. OPTIMIZATION

Consider the simple air core stimulator shown in Fig. 4. One quarter of the problem is displayed. The “C” shaped block can be considered the mandrel for the coil. This shape is chosen because it will be treated as a shell for the first part of the analysis,

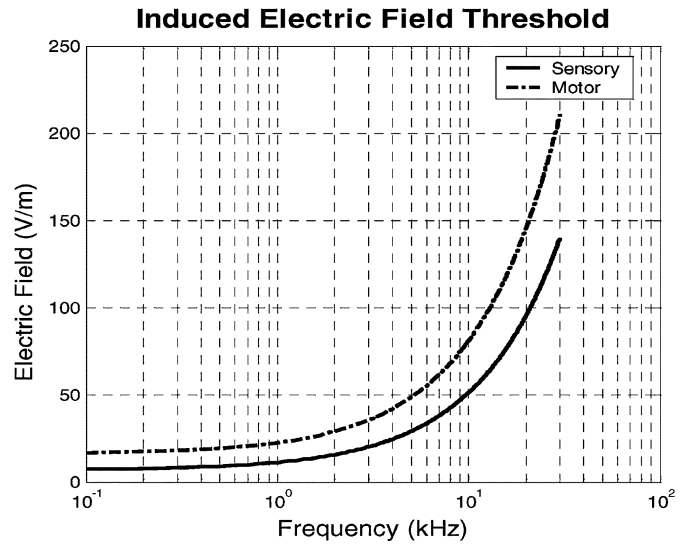


Fig. 3. Neural stimulation threshold as a function of frequency.

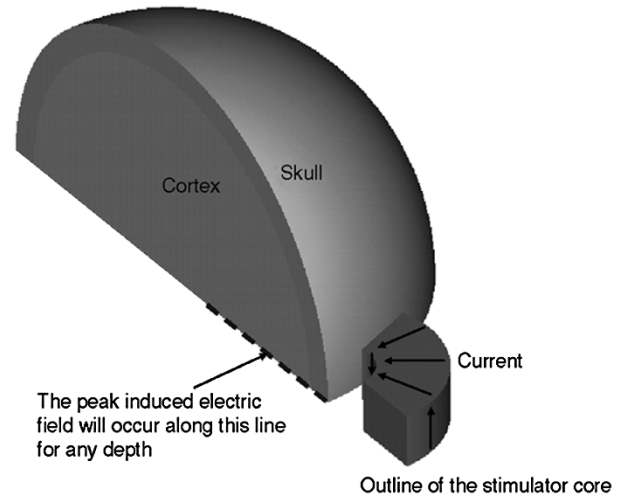


Fig. 4. Stimulator core next to the brain in quarter plane perspective.

and then filled with steel using a tape wound core for the second part. A typical induced electric field pattern is shown in Fig. 5. The peak field occurs along the center axis of the core.

What constitutes an optimized system? Among the items that might be optimized are the following:

- capacitor size;
- core stimulator size;
- voltage;
- energy.

Energy involves both the capacitor and the voltage. The number of turns N increases the resistance, and lowers the peak current in (4).

A. Air Core

An air core optimization is simplest. Many finite-element and boundary-element programs are suitable for analyzing this type of problem. Since the air core represents a linear analysis, a three-dimensional boundary-element analysis [7] is employed to predict the electric field as a function of depth for various core sizes.

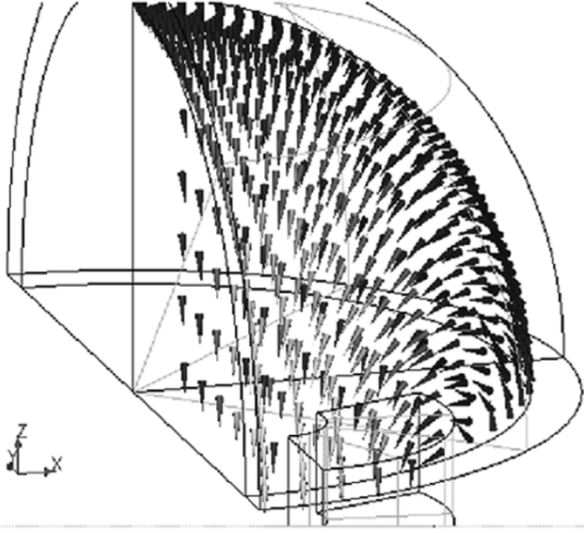


Fig. 5. Induced electric field arrow plot.

1) *Analytic Optimization:* Consider an air core in which energy is to be minimized, and the core shape is known. If the shape in Fig. 4 is known, then the problem can be solved using a numerical solver for the induced field E_0 at desired depth, at current I_0 and radian frequency ω_0 . The actual induced electric field will scale from this value by the number of turns N , the actual peak current I_p , and the frequency ω

$$E = NE_0 \left(\frac{I_p}{I_0} \right) \cdot \left(\frac{\omega}{\omega_0} \right). \quad (6)$$

The induced electric field is required to satisfy the requirement dictated in (5); this can be interpreted as a requirement on voltage V

$$V = NI_0 \left(\frac{\omega_0}{\omega} \right) \left(\frac{\beta(1 + \gamma\omega/\pi)}{E_0} \right) e^{-\left(\frac{\tan^{-1}(\frac{\omega}{\alpha})}{\omega/\alpha} \right)} \sqrt{\frac{L}{C}}. \quad (7)$$

Let L_0 represent the inductance of the core with one turn. The resistance is actually a bit complicated because it must account for that lost in the thyristor and the wire. As will be seen shortly, it must also account for the eddy and hysteresis loss in the core if it is magnetizable. For the moment consider only the loss from the wire, and consider the core to be filled with wire so that additional turns are added at the expense of a smaller cross section. In this approximation, the inductance and resistance will scale as N^2

$$\begin{aligned} L &= N^2 L_0 \\ R &= N^2 R_0. \end{aligned} \quad (8)$$

The energy can be written in terms of the two remaining unknowns C and N as

$$W = \frac{1}{2} L_0 I_0^2 \left(\frac{\omega_0}{\omega} \right)^2 \left(\frac{\beta(1 + \gamma\omega/\pi)}{E_0} \right)^2 e^{-2 \left(\frac{\tan^{-1}(\frac{\omega}{\alpha})}{\omega/\alpha} \right)}. \quad (9)$$

Consider the one turn air core stimulator shown in Fig. 4. The inductance is $0.004 \mu\text{H}$ for an ID = 3.214 cm, OD = 10.66

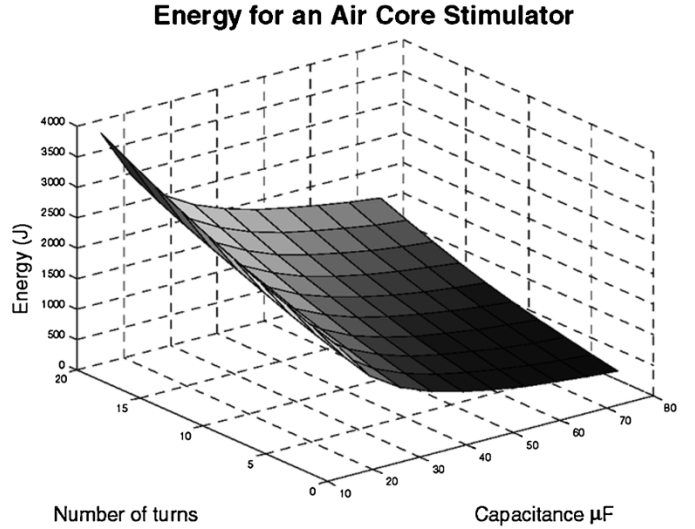


Fig. 6. Energy required for stimulation at a depth of 1 cm for a spread of capacitance and turns options.

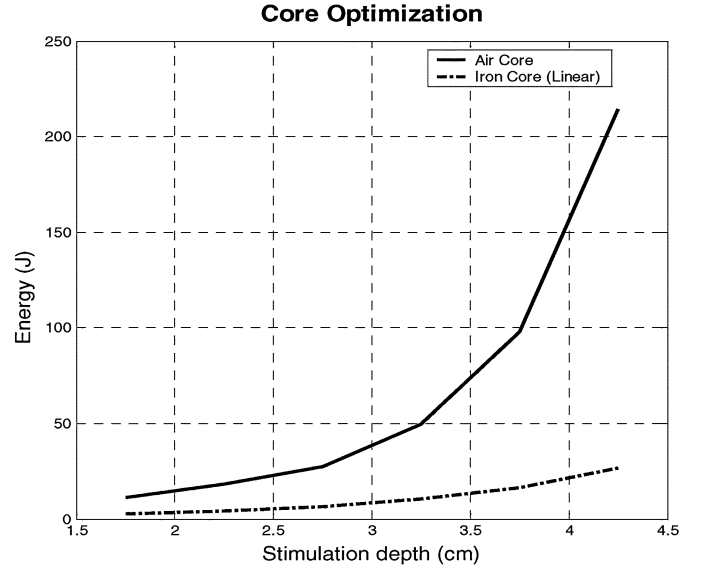


Fig. 7. Optimized energy as a function of various stimulation depths.

cm, and height = 5.9 cm. The core induces an electric field of 4.273 mV/m with 1 A of excitation with characteristic frequency 5.208 kHz. Using these parameters in (9) yields the energy requirement shown in Fig. 6 for a spread of capacitance values and number of turns. The equations clearly suggest the use of a small number of turns and a large capacitor. As will be seen shortly, when more realistic relationships are employed to relate resistance and inductance to the number of turns by incorporating parasitic lead inductance and resistance loss from the thyristor and core, this trend will change.

2) *Numerical Optimization:* When the problem is considered as a four-parameter optimization in the variables C , V , N , and core size x , it can no longer be solved analytically. A numerical approach allows the parameters such as resistance to be treated more realistically, with the inclusion of proper bounds on voltage. Assume the core size to be a scale parameter x , scaling all the dimensions equally from the core origin. If ζ_0 represents

TABLE II
OPTIMIZATION RESULTS FOR AN AIR CORE STIMULATOR

Stimulation Depth (cm)	Scale Parameter	Capacitance (μF)	Voltage (kV)	Number of Turns	Frequency (kHz)	Stimulation Current (kA)
1.75	1.162	5	2.136	18	26.3319	30.6324
2.25	1.391	5	2.689	18	24.9194	36.3856
2.75	1.675	6.105	3	18	21.2232	41.8804
3.25	1.75	10.98	3	18	15.5839	54.3823
3.75	1.75	21.77	3	18	11.0567	74.5978
4.25	1.75	47.62	3	18	7.4599	105.7719

the length of the core winding with one turn, then the length ζ of the winding with N turns, scaled by a value x is

$$\zeta = Nx\zeta_0. \quad (10)$$

The combined resistance of both the parasitic core resistance and the diode R_0 with one turn is about 20 m Ω . A reasonable approximation to the resistance to be used in (2) is

$$R = R_0 \left(0.9 + 0.1 \frac{\zeta}{\zeta_0} \right). \quad (11)$$

The leads have a parasitic inductance $L_{\text{Parasitic}}$ equal to about 3 μH . Allow the core to vary through a spread of sizes and compute the inductance as the flux linkage per amperage for each size $L_0(x)$. The inductance with N turns is

$$L = N^2 L_0(x) + L_{\text{Parasitic}}. \quad (12)$$

Compute the induced electric field $E_0(x)$ with a current of I_0 A at radian frequency ω_0 for a spread of stimulation depths. Equation (6) dictates the induced electric field as delivered by the stimulator. If the inductance and induced electric field E_0 are fitted to the core size using a smooth spline, its derivative can be approximated and a variable metric procedure can be used to minimize an optimization index. If a combination of energy and stimulator core size are involved in the design objective, the optimization problem becomes

$$\begin{aligned} \text{Min } \mathfrak{S} &= \frac{1}{2} CV^2 x \\ \text{Subject to } NE_0 \left(\frac{I_p}{I_0} \right) \cdot \left(\frac{\omega}{\omega_0} \right) &= \beta \left(1 + \frac{\gamma\omega}{\pi} \right). \end{aligned} \quad (13)$$

The peak stimulator current I_p is determined from (4). This index is one of many options open to the designer. One of the applications motivating this research was the use of these stimulators in the field for alertness assistance. In such mobile contexts, minimizing size and energy consumption is warranted.

a) Optimization Algorithm: A word about the approach for this constrained optimization procedure is in order. Trust region algorithms are applicable, and the problem has strong local convergence. The basic idea is to approximate the problem to be minimized with a simpler function which reasonably reflects the behavior of real functional in a neighborhood near the solution sought [8]. This neighborhood is the trust region. Normally one step is taken to minimize the functional in question. A piecewise reflective search can be conducted at each iteration

[9]. Sequential quadratic programming techniques have outperformed every other nonlinear optimization algorithm in terms of efficiency, accuracy, and percentage of successful solutions over a large range of test problems [10]. To quote the documentation from Matlab's algorithm documentation:

“Based on the work of Biggs [11], Han [12], and Powell ([13], [14]), the method allows you to closely mimic Newton's method for constrained optimization just as is done for unconstrained optimization. At each major iteration, an approximation is made of the Hessian of the Lagrangian function using a quasi-Newton updating method. This is then used to generate a QP subproblem whose solution is used to form a search direction for a line search procedure. An overview of SQP is found in Fletcher [15], Gill *et al.* [16], Powell [17], and Schittkowski [18].”

3) Results of the Air Core Numerical Optimization: Stimulation depth is a key parameter in the optimization. Fig. 7 shows how the system energy changes with target stimulation depth. Here, a core shell with ID = 1.836 cm, OD = 6.096 cm, and height = 3.38 cm is scaled in all dimensions by a scale factor which varied from 1 to 1.75. The capacitance was allowed to vary from 5 to 75 μF , the voltage from 500 V to 3 kV, and the number of turns from 2 to 18. The problem has many local minima. A Monte Carlo method is employed to randomly vary the starting guess to increase the probability that the global minimum is found.

Table II shows the results of the optimization for each of the parameters. Among the key lessons are the following.

- Smaller cores are desired for the lower stimulation depths.
- Deeper stimulation target depths drive both the capacitance and the voltage up. The voltage comes up slower since it affects the optimization by its square.
- When parasitic losses such as the switching and lead resistance are considered, the optimization always favors a higher number of turns. The neural response depicted in Fig. 3 is driving the frequency down with depth, and the inductance up.

B. Steel Core

Tape wound cores substantially reduce the required system size and energy requirements [19], [20], although their construction is more difficult [21]. The advantage is introduced with the price that the problem is nonlinear. The nonlinear element complicates the optimization in two respects. First, (2) no longer describes the current. The magnitude will be dictated by the degree

TABLE III
OPTIMIZATION PARAMETERS FOR A LINEAR IRON CORE STIMULATOR USING $\mu_r = 1000$

Stimulation Depth (cm)	Scale Parameter	Capacitance (μF)	Voltage (kV)	Number of Turns	Frequency (kHz)	Stimulation Current (kA)
1.75	1.0022	5	1.0616	17.9702	13.7545	8.0951
2.25	1.2508	5	1.2975	15.2522	14.4552	8.8111
2.75	1.3283	5	1.6264	14.5454	14.4532	10.5291
3.25	1.3579	5	2.0476	14.334	14.4539	13.0631
3.75	1.3738	5	2.575	14.2388	14.4533	16.3166
4.25	1.3913	5.9533	3	13.7745	13.558	20.4981

of saturation. Second, the frequency is no longer a simple index. A core in saturation is characterized by a higher frequency and a lower amplitude. A Fourier decomposition must be performed to determine the fundamental frequency amplitude and at least the first harmonic.

1) *Linear*: Much is to be learned by examining what should be expected from a steel core. The gap is very large. Treating the core as linear with a relative permeability of 1000 is a reasonable approximation. Fig. 7 shows how the energy drops with steel core in this approximation. Since the inductance is so high, the optimization parameters take a different posture. As shown in Table III, important trends with iron cores are the following.

- Deeper stimulation target depths require larger cores as with air cores.
- Because of the high inductance, low capacitance is desirable.
- As with air cores, voltage must increase with target stimulation depth.
- Deeper target depths are commensurate with lower stimulation frequencies, and a lower frequency.
- The required stimulation current increases nearly linearly with depth ($4.25/1.75 = 2.43$; $20.49/8.09 = 2.53$). By contrast, the required air core amp-turn excitation increases by $105.7/30.6 = 3.45$. The iron core field does not fall off as rapidly with distance.

2) *Saturable Cores*: The analysis becomes nonlinear with real magnetizable cores. The inductance of the core is computed using a numerical analysis routine for a spread of excitation current.

The equations governing the current in the *RLC* circuit are

$$\frac{d\lambda}{dt} + RI + \frac{1}{C} \int I dt = 0 \quad (14)$$

where the core flux linkage $\lambda = L \cdot I$, and L is a function of current I . To determine $L(I)$, the core is excited through a spread of current, and the flux computed for each excitation. The governing equation is

$$\left(L + I \frac{dL}{dI} \right) \frac{d^2 I}{dt^2} + \left(2 \frac{dL}{dt} + I \frac{d^2 L}{dI^2} \right) \left(\frac{dI}{dt} \right)^2 + R \frac{dI}{dt} + \frac{I}{C} = 0. \quad (15)$$

The flux has two components of change, one due to the changing current, and the second due to the changing inductance. A Runge-Kutta-Fehlberg technique based on the

B-H Curve for Grain Oriented Steel

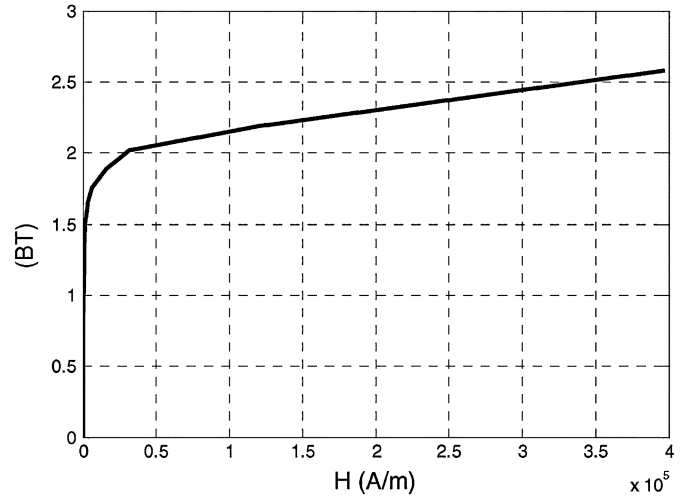


Fig. 8. $B-H$ curve for the 3% grain-oriented steel used for the steel.

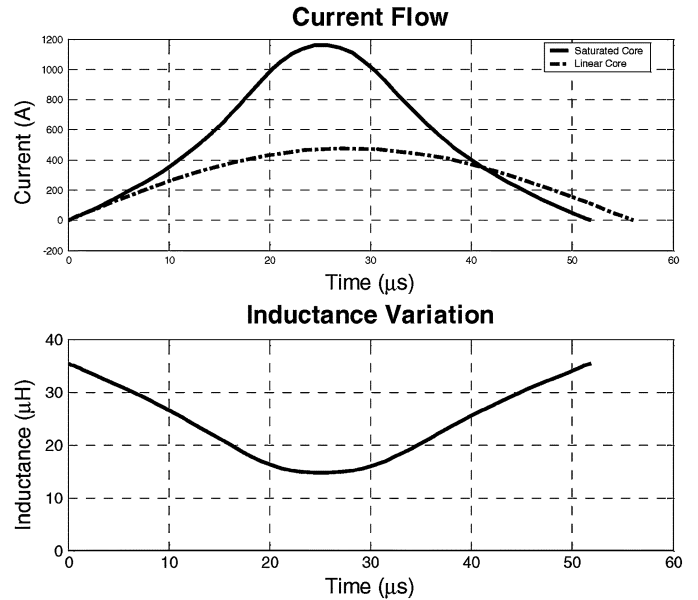


Fig. 9. Current and inductance as a function of time for a nonlinear core.

Dormand Prince pair [22], [23] was employed to integrate this equation numerically. Assume a scale parameter of 1.25, a capacitance of $15 \mu\text{F}$, a 12-turn coil, and a 3% grain-oriented steel with initial relative permeability of 1500. Fig. 8 shows the saturation characteristics for this steel.

TABLE IV
RESULTS FOR A NONLINEAR CORE ANALYSIS

Target Depth (cm)	Scale Parameter	Capacitance (μF)	Voltage (kV)	Number of Turns	Frequency (kHz)	Stimulation Current (kA)	Energy (J)
1.75	1.7167	15.8764	0.4206	13.655	6.2797	1.4495	1.4041
2.25	1.75	35	0.4	13.984	4.0998	2.0442	2.8002
2.75	1.5021	34.9972	0.4002	18	3.54	2.3122	2.8027
3.25	1.75	34.9537	0.5752	18	3.2554	3.3454	5.7818
3.75	1.75	34.9579	0.6896	18	3.2552	4.0112	8.3118
4.25	1.75	34.9994	0.8136	18	3.2533	4.7351	11.583

TABLE V
RESULTS FOR THE NONLINEAR CORE ANALYSIS AFTER DOUBLING THE RHEOBASE AND CHRONAXIE VALUES

Target Depth (cm)	Scale Parameter	Capacitance (μF)	Voltage (kV)	Number of Turns	Frequency (kHz)	Stimulation Current (kA)	Energy (J)
1.75	1.7353	34.9637	1.0384	17.867	3.2801	5.685	18.851
2.25	1.747	27.5194	1.3949	18	3.6591	6.8373	26.772
2.75	1.75	27.176	1.75	18	3.7858	8.3957	41.613
3.25	1.75	62.4074	1.75	18	2.772	13.5831	95.561
3.75	1.7501	112.4891	1.75	18	1.794	27.2075	172.25
4.25	1.7502	207.656	1.75	18	1.342	45.9637	317.97

The current for the nonlinear core is shown in Fig. 9. As anticipated by (2), the time period has dropped, consistent with the lower inductance during excitation. Second, and more important, shoulders appear on the current waveform, and the current increases dramatically at midpoint. This distorted waveform with higher current is the earmark of a core in saturation. The linear core current, shown as a dashed line, has a larger inductance and a longer time period. The inductance follows the profile in the lower trace in Fig. 9.

Table IV shows the results of the nonlinear analysis allowing the capacitance to vary from 5 to 35 μF , the number of turns from 1 to 18, the voltage from 400 V to 1.5 kV, and the core scale parameter from 1 to 1.75, using a parasitic inductance of 4.5 μH .

A least square curve fit routine is used to determine the fundamental component of the peak current and the frequency ω . Since the electric field is computed *a priori* for a range of current at a fixed frequency ω_0 , a spline is used correlate the circuit delivered amp-turn peak with the field theory computed E field. As far as the field analysis program is concerned, the core is excited at the fundamental amplitude. The numerical field analysis is solved only at frequency ω_0 . This E field must be scaled by the ratio of the circuit frequency as dictated by the zero crossing to the field analysis frequency, ω/ω_0 .

3) *Cortical Stimulation*: The results quoted are consistent with the strength duration information of Table I, and dependent on the optimization criteria targeted which could in general be different from (13). Peripheral nerves are myelinated, whereas cortical nerves are not. The myelin sheath will increase both β and γ in Table I. Geddes shows some of the variation of γ in [24]. More reasonable values of β and γ for the cortex are suggested by this team to be 32 V/m and 406 μs , and yield the optimization results in Table V. Doubling these parameters from their former values in Table I increases the energy by more than an order of magnitude. Until data analogous to Table I is available for

the cortex, the higher values of 32 V/m and 406 μs for β and γ appear reasonable, since they are consistent with excitation levels in the laboratory.

IV. CONCLUSION

A method is presented for optimizing a magnetic stimulation system. The frequency, system voltage, capacitance, core stimulator size, and the number of turns are treated as unknowns. Based on the neural magnetic stimulation response parameters, and the electric field as computed through a boundary element solver, the ideal parameters for the system can be derived. A trust region technique is used to solve the four-parameter optimization problem. The result is target depth dependent, and certainly dependent on the shape of the stimulation coil. Deeper targets are commensurate with lower excitation frequency, and higher amp-turn products. Rheobase and chronaxie values of 32 V/m and 406 μs appear consistent with laboratory data.

REFERENCES

- [1] K. Hsu, S. Nagarajan, and D. Durand, "Analysis and efficiency of magnetic stimulation," *IEEE Trans. Biomed. Eng.*, vol. 50, no. 11, pp. 1276–1285, Nov. 2003.
- [2] P. Ravazzani, G. Tognola, J. Ruohonen, and F. Grandori, "Frequency related effects and geometrical characteristics," in *Proc. 22nd Annu. EMBS Int. Conf.*, Chicago, IL, Jul. 23–28, 2000, pp. 2625–2628.
- [3] T. Onuki, S. Wakao, T. Miyokawa, and Y. Nishimura, "Design optimization of simulation coil system for nerve stimulation," *IEEE Trans. Magn.*, vol. 34, no. 4, pp. 2159–2161, Jul. 1998.
- [4] K. H. Hsu and D. Durand, "A 3D differential coil design for localizing magnetic stimulation," *IEEE Trans. Biomed. Eng.*, vol. 48, pp. 1162–1168, Oct. 2001.
- [5] N. Al-Mutawaly and R. Findlay, "A novel coil design for magnetic nerve stimulation," in *IEEE Canadian Conf. Electrical and Computer Engineering*, vol. 2, May, 24–28 1998, pp. 669–672.
- [6] J. D. Bourland, J. A. Nyenhuis, W. A. Noe, J. D. Schaefer, K. S. Foster, and L. A. Geddes, "Motor and sensory strength-duration curves for MRI gradient fields," in *Proc. Int. Soc. Magnetic Resonance in Medicine 4th Scientific Meeting and Exhibit*, New York, 1996, p. 1724.

- [7] D. Zheng, "Three dimensional eddy current analysis by the boundary element method," *IEEE Trans. Magn.*, vol. 33, no. 2, pp. 1354–1357, Mar. 1997.
- [8] J. J. Moré and D. C. Sorensen, "Computing a trust region step," *SIAM J. Sci. Stat. Comput.*, vol. 3, pp. 553–572, 1983.
- [9] T. F. Coleman and Y. Li, "A reflective Newton method for minimizing a quadratic function subject to bounds on some of the variables," *SIAM J. Opt.*, vol. 6, no. 4, pp. 1040–1058, 1996.
- [10] K. Schittkowski, "NLQPL: A FORTRAN-subroutine solving constrained nonlinear programming problems," *Ann. Oper. Res.*, vol. 5, pp. 485–500, 1985.
- [11] M. C. Biggs, "Constrained minimization using recursive quadratic programming," in *Toward Global Optimization*, L. C. W. Dixon and G. P. Szergo, Eds. Amsterdam, The Netherlands: North-Holland, 1975, pp. 341–349.
- [12] S. P. Han, "A globally convergent method for nonlinear programming," *J. Opt. Theory Appl.*, vol. 22, p. 297, 1977.
- [13] M. J. D. Powell, "The convergence of variable metric methods for nonlinearly constrained optimization calculations," in *Nonlinear Programming 3*, O. L. Mangasarian, R. R. Meyer, and S. M. Robinson, Eds. New York: Academic, 1978.
- [14] —, "A fast algorithm for nonlinearly constrained optimization calculations," in *Numerical Analysis, Lecture Notes in Mathematics*, G. A. Watson, Ed. New York: Springer-Verlag, 1978, vol. 630.
- [15] R. Fletcher, "Practical methods of optimization," in *Unconstrained Optimization*. New York: Wiley, 1980, vol. 1.
- [16] P. E. Gill, W. Murray, and M. H. Wright, *Practical Optimization*. London, U.K.: Academic, 1981.
- [17] M. J. D. Powell, "Variable metric methods for constrained optimization," in *Mathematical Programming: The State of the Art*, A. Bachem, M. Grotschel, and B. Korte, Eds. New York: Springer-Verlag, 1983, pp. 288–311.
- [18] W. Hock and K. Schittkowski, "A comparative performance evaluation of 27 nonlinear programming codes," *Computing*, vol. 30, p. 335, 1983.
- [19] K. R. Davey, C. H. Cheng, and C. M. Epstein, "An alloy—CORE electromagnet for transcranial brain stimulation," *J. Clin. Neurophys.*, vol. 6, no. 4, p. 365, 1989.
- [20] C. M. Epstein and K. R. Davey, "Iron-core coils for transcranial magnetic stimulation," *J. Clin. Neurophys.*, vol. 19, no. 4, pp. 376–381, Dec. 2002.
- [21] K. Davey and C. M. Epstein, "Magnetic stimulation coil and circuit design," *IEEE Trans. Biomed. Eng.*, vol. 47, no. 11, pp. 1493–1499, Nov. 2000.
- [22] G. Forsythe, M. Malcolm, and C. Moler, *Computer Methods for Mathematical Computations*. Englewood Cliffs, NJ: Prentice-Hall, 1977.
- [23] D. Kahaner, C. Moler, and S. Nash, *Numerical Methods and Software*. Englewood Cliffs, NJ: Prentice-Hall, 1989.
- [24] L. A. Geddes, "Chronaxie," *Austral. Phys. Eng. Sci. Med.*, vol. 22, no. 1, p. 17, 1999.